Electronic Supplementary Material (ESI) for Physical Chemistry Chemical Physics.
This journal is © the Owner Societies 2023

Electronic Supplementary Information (ESI)

ESI 1. Details on full-field nano-XAFS measurements

Table S1. The energy list of full-field nano-XAFS measurements

Block	Energy range /eV	Energy space /eV	Number of the energy point	Exposure time /s
1	7000－7090	10	10	10
2	7100－7134.65	0.35	100	10
3	7135－7159	1	25	10
4	7160－7200	2.67	15	10

ESI 2. Details on Analysis of full-field nano-XAFS spectra

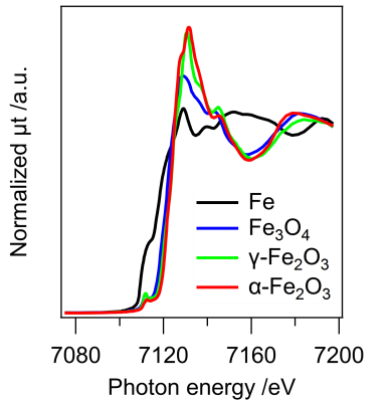

Figure S1. Fe *K*-edge XAFS spectra of Fe standard samples for XANES analysis.

Scheme S1. Analysis of spatially resolved Fe *K*-edge XAFS for dendritic FeO_x and Cr-FeO_x

Linear combination fitting (LCF) equation of spatially resolved XAFS

$$\mu(x,y,E) = \underbrace{\epsilon_0(x,y,E) + \epsilon_1(x,y)\cdot(E-E_0)}_{\text{background}} + \underbrace{c_{Fe_3O_4}(x,y)\mu_{Fe_3O_4}(E)}_{Fe_3O_4} + \underbrace{c_{\gamma\text{-}Fe_2O_3}(x,y)\mu_{\gamma\text{-}Fe_2O_3}(E)}_{\gamma\text{-}Fe_2O_3} + \underbrace{c_{\alpha\text{-}Fe_2O_3}(x,y)\mu_{\alpha\text{-}Fe_2O_3}(E)}_{\alpha\text{-}Fe_2O_3}$$

$E_0 = 7111.2\ eV$ $\quad \mu_{Fe_3O_4}(E),\ \mu_{\gamma\text{-}Fe_2O_3}(E),\ \mu_{\alpha\text{-}Fe_2O_3}(E)$: standard Fe K-edge XANES spectra of Fe_3O_4, γ-Fe_2O_3, and α-Fe_2O_3

Estimation of Fe chemical state parameters

Fe density: $\rho(x,y) = c_{Fe_3O_4}(x,y) + c_{\gamma\text{-}Fe_2O_3}(x,y) + c_{\alpha\text{-}Fe_2O_3}(x,y)$

Fe valence: $v(x,y) = \dfrac{\frac{8}{3}c_{Fe_3O_4}(x,y) + 3\{c_{\gamma\text{-}Fe_2O_3}(x,y) + c_{\alpha\text{-}Fe_2O_3}(x,y)\}}{\rho(x,y)}$

FeO_x pahse proportion: $\boldsymbol{\eta}(\boldsymbol{x},\boldsymbol{y}) = \left(\eta_{Fe_3O_4}(x,y), \eta_{\gamma\text{-}Fe_2O_3}(x,y), \eta_{\alpha\text{-}Fe_2O_3}(x,y)\right)$

$$= \left(\frac{c_{Fe_3O_4}(x,y)}{\rho(x,y)}, \frac{c_{\gamma\text{-}Fe_2O_3}(x,y)}{\rho(x,y)}, \frac{c_{\alpha\text{-}Fe_2O_3}(x,y)}{\rho(x,y)}\right)$$

Probability density (kernel density) estimation

$$\boldsymbol{\mu} = \begin{pmatrix} c_{Fe_3O_4} \\ c_{\gamma\text{-}Fe_2O_3} \\ c_{\alpha\text{-}Fe_2O_3} \end{pmatrix} = \begin{pmatrix} \eta_{Fe_3O_4} \\ \eta_{\gamma\text{-}Fe_2O_3} \\ \eta_{\alpha\text{-}Fe_2O_3} \end{pmatrix}\rho = \boldsymbol{\eta}\rho$$

- Kernel density for 1 pixel

$$p_i(\boldsymbol{\mu}) = \mathcal{N}(\boldsymbol{\mu_i}, \boldsymbol{\Sigma_i}) = \frac{1}{(2\pi)^{\frac{3}{2}}\sqrt{|\boldsymbol{\Sigma_i}|}}\exp\left\{-\frac{1}{2}{}^t(\boldsymbol{\mu}-\boldsymbol{\mu_i})\boldsymbol{\Sigma_i^{-1}}(\boldsymbol{\mu}-\boldsymbol{\mu_i})\right\}$$
$$= \frac{1}{(2\pi)^{\frac{3}{2}}\sqrt{|\boldsymbol{\Sigma_i}|}}\exp\left\{-\frac{1}{2}{}^t(\boldsymbol{\eta}\rho-\boldsymbol{\mu_i})\boldsymbol{\Sigma_i^{-1}}(\boldsymbol{\eta}\rho-\boldsymbol{\mu_i})\right\}$$
$$= p_i(\boldsymbol{\eta},\rho)$$

$\boldsymbol{\mu_i} = \begin{pmatrix} a_i \\ b_i \\ c_i \end{pmatrix}$:estimated value of LCF $\qquad$ $\boldsymbol{\Sigma_i}$: covariation matrix of LCF (3×3)

- Kernel density in$(\rho,\boldsymbol{\eta})$-space

$$P(\rho,\boldsymbol{\eta}) = \frac{1}{N}\sum_{i=0}^{N-1} p_i(\rho,\boldsymbol{\eta})$$

- Kernel density in $\boldsymbol{\eta}$-space

$$P(\boldsymbol{\eta}) = \frac{1}{N}\int_0^\infty \sum_{i=0}^{N-1} p_i(\rho,\boldsymbol{\eta})\rho^2 d\rho$$

Discussion on the validity of the linear combined curve-fitting analysis

To confirm the validity of this three-phase linear combined fitting analysis, we have conducted principal component analysis (PCA) to the all valid spatially-resolved XAFS data in the FeO_x and Cr-FeO_x particles in this paper, after background removal, normalization, and data centering by subtracting the average XAFS of all pixels. The cumulative contribution in PCA for up to 20 elements showed that above 5 elements exceeded 50% (Figure S2a). Then, we have conducted multivariate curve resolution alternating least squares (MCR-ALS) analysis on 20 spectral elements, with the difference spectra of the three phases (Fe_3O_4, γ-Fe_2O_3, and α-Fe_2O_3) as the initial values of the spectral matrix, showed that the structure according three phases remain roughly in the first three elements (Figure S2bc). The rest of the spectra components in Figure S2b do not attribute to essential XAFS characteristics, but rather structure before the edge around 7100－7120 eV. They could be associated with components corresponding to remnants of background, distortions in the illumination light field, or artifacts from FZP imaging. These contributions to the background structure near the pre-edge may correspond to elements with cumulative contributions exceeding 50% in the PCA other than the main components of Fe_3O_4, γ-Fe_2O_3, and α-Fe_2O_3. The concentration matrix obtained from the MCR-ALS analysis was found to be in good agreement with the phase distribution described in this paper, indicating the validity of this curve-fitting analysis.

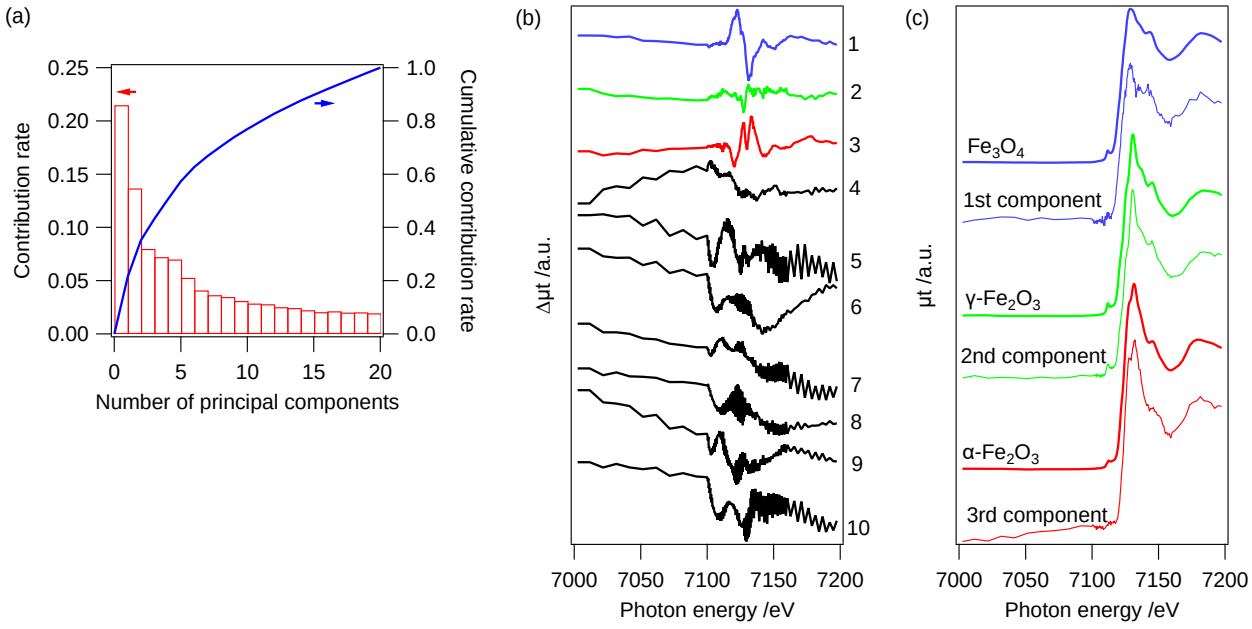

Figure S2. (a) The contribution (red) and cumulative contribution (blue) rates of the PCA analysis up to 20 components. (b) The difference spectra (Δμt) of the first 10 components of the MCR-ALS analysis, and (c) the XANES spectra of the three reference compounds of Fe_3O_4, γ-Fe_2O_3, and α-Fe_2O_3 and those estimated by the summation of the average spectrum and the difference spectrum of the 1st/2nd/3rd component. These XANES spectra of the three components were similar to those of the reference compounds.

ESI 3. Details on full-field nano-XAFS spectra analysis results

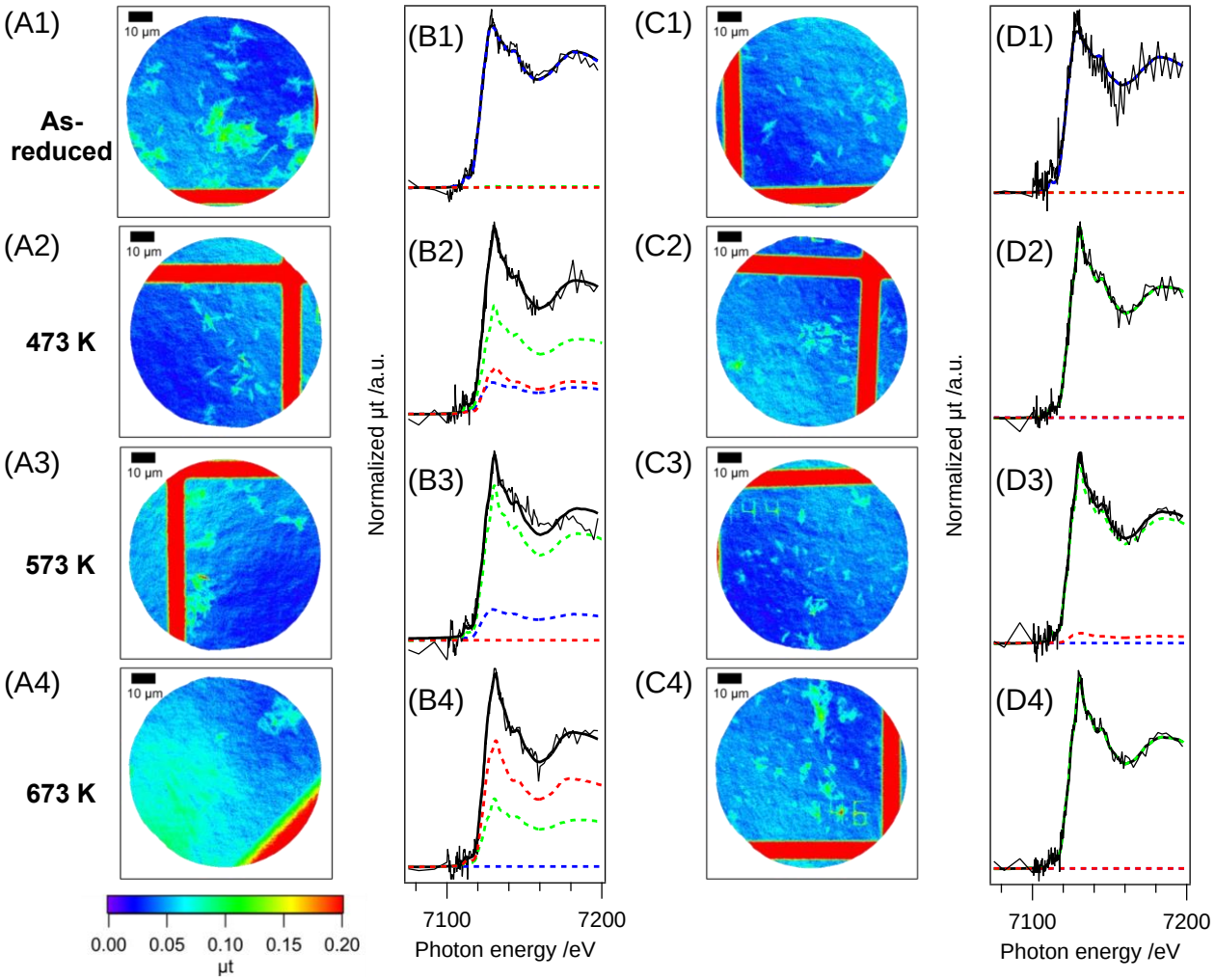

Figure S3. (A, C) Full-field absorption images at 7.130 keV and (B, D) integrated XAFS spectra of the particle regions in the full-field images for (A, B) dendritic FeO_x and (C, D) dendritic 10 wt% Cr-FeO_x (1) as reduced, and after oxidation at (2) 473, (3) 573, and (4) 673 K. Black solid lines in B, D: observed data; black bold lines in B, D: linear combination fitting data; blue dashed bold lines in B, D: Fe_3O_4 phase fraction; green dashed bold lines in B, D: γ-Fe_2O_3 phase fraction; red dashed bold lines in B, D: α-Fe_2O_3 phase fraction.

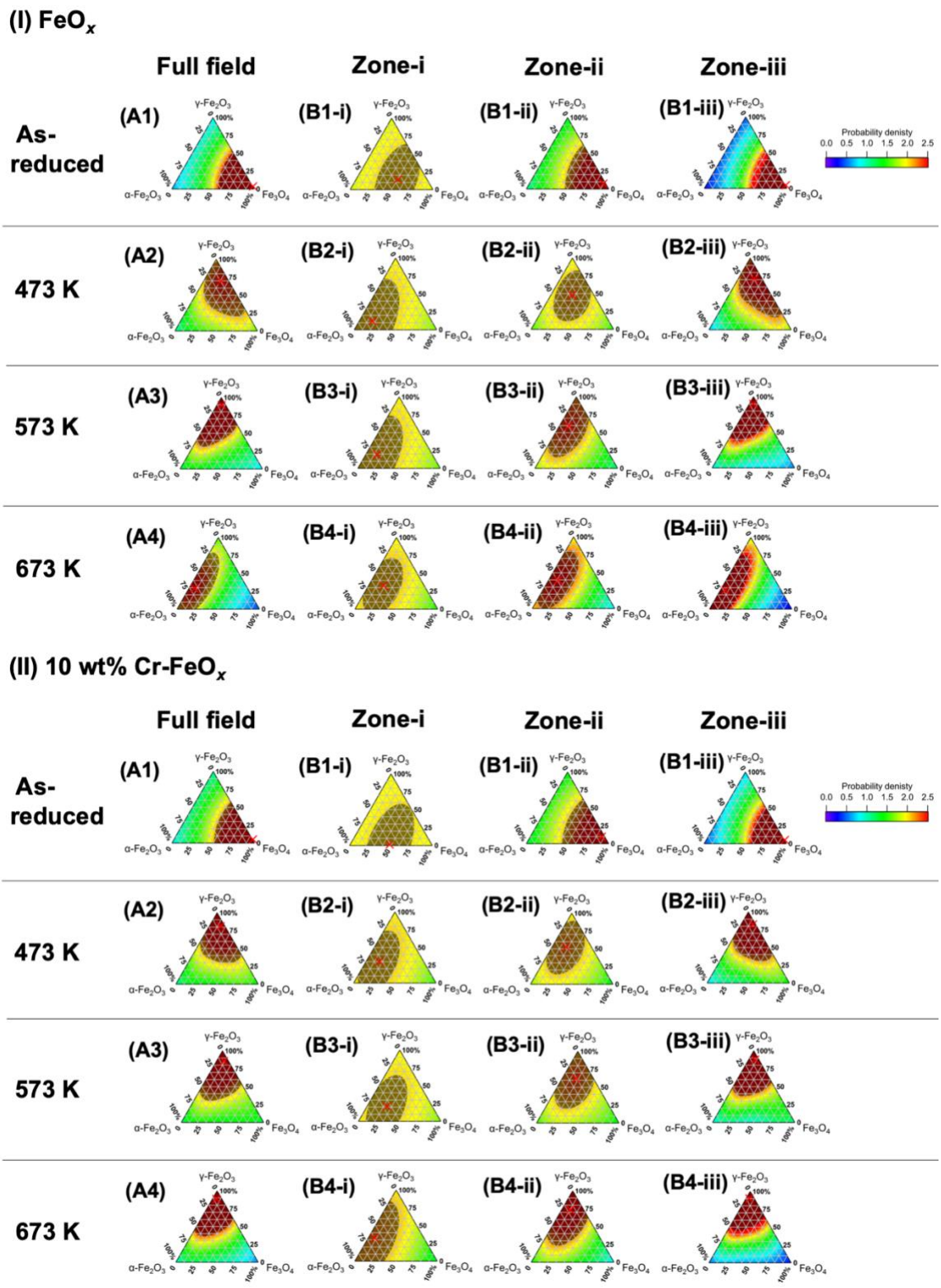

Figure S4. (A) Ternary probability density diagrams of the Fe phases and (B) ternary posterior probability density diagrams in specific Fe density ($\Delta\mu t$) range zones (i)–(iii) of (I) dendritic FeO_x particles and (II) dendritic 10 wt% Cr-FeO_x particles, which are the same as in Figs. 5A and C and 6A and C. Maximum probability density points (×) and probable 50% phase proportion area are shown in transparent black. (1) As-reduced and after oxidation at (2) 473 K, (3) 573 K, and (4) 673 K.

Table S2. Maximum probability density $P(\eta_{max})$, maximum posterior probability density $p(\eta_{max}|$(i), (ii), or (iii)), and Fe phase proportion coordinates at the maxima (η_{max}) in the ternary diagrams in Figs. 5 and 6

Sample	Condition	Full-field		Zone-(i)		Zone-(ii)		Zone-(iii)	
		$P(\eta_{max})$	η_{max} %	$P(\eta_{max}\|$(i))	η_{max} %	$P(\eta\|$(ii))	η_{max} %	$P(\eta_{max}\|$(iii))	η_{max} %
Dendritic FeO_x	As-reduced	7.462	(96,0,4)	2.071	(51,12,37)	3.228	(90,6,4)	10.546	(96,4,0)
	Oxidation at 473 K	2.423	(21,68,11)	2.083	(16,12,72)	2.175	(25,47,29)	2.6356	(20,71,9)
	Oxidation at 573 K	4.011	(6,89,5)	2.093	(14,18,68)	2.409	(11,59,30)	5.119	(5,89,6)
	Oxidation at 673 K	2.243	(7,28,65)	2.115	(18,29,53)	2.518	(11,39,50)	3.521	(6,26,68)
Dendritic 10 wt % Cr-FeO_x	As-reduced	5.031	(95,5,0)	2.055	(47,1,52)	2.815	(86,9,5)	7.317	(96,4,0)
	Oxidation at 473 K	2.883	(14,81,5)	3.060	(16,29,55)	2.219	(16,52,32)	3.250	(14,82,4)
	Oxidation at 573 K	3.519	(9,85,6)	2.068	(24,20,56)	2.310	(15,62,23)	4.053	(8,87,5)
	Oxidation at 673 K	4.332	(4,88,8)	2.268	(7,32,61)	2.709	(10,73,17)	5.900	(4,90,6)

Fe phase proportion coordinates are defined as $\boldsymbol{\eta} = (\eta_{Fe3O4}, \eta_{\gamma\text{-}Fe2O3}, \eta_{\alpha\text{-}Fe2O3})$, where η_{Fe3O4}, $\eta_{\gamma\text{-}Fe2O3}$, and $\eta_{\alpha\text{-}Fe2O3}$ are proportions of the Fe_3O_4, γ-Fe_2O_3, and α-Fe_2O_3 phases, respectively.